

Electromagnetic sunscreen model: implementation and comparison between several methods: step-film model, differential method, Mie scattering, and scattering by a set of parallel cylinders

Marie Lécureux,^{1,2,*} Stefan Enoch,² Carole Deumié,² and Gérard Tayeb²

¹Naos Recherche, Aix-en-Provence 13856, France

²Aix-Marseille Université, CNRS, Centrale Marseille, Institut Fresnel, UMR 7249, Marseille 13013, France

*Corresponding author: marie.lecureux@fresnel.fr

Received 28 May 2014; accepted 9 August 2014;
posted 26 August 2014 (Doc. ID 212945); published 30 September 2014

Sunscreens protect from UV radiation, a carcinogen also responsible for sunburns and age-associated dryness. In order to anticipate the transmission of light through UV protection containing scattering particles, we implement electromagnetic models, using numerical methods for solving Maxwell's equations. After having our models validated, we compare several calculation methods: differential method, scattering by a set of parallel cylinders, or Mie scattering. The field of application and benefits of each method are studied and examples using the appropriate method are described. © 2014 Optical Society of America

OCIS codes: (290.0290) Scattering; (290.2200) Extinction; (290.4020) Mie theory; (290.5825) Scattering theory; (290.5850) Scattering, particles.
<http://dx.doi.org/10.1364/AO.53.006537>

1. Introduction

UV radiation can penetrate into skin and trigger vitamin D_3 synthesis [1] useful to skeletal maintenance. On the contrary, too much exposure is a carcinogen [2] (radiation induces DNA mutations). Skin cancers affect more than 1.5 million Americans each year [3] and sunscreens are widely used to protect against radiation risks.

In order to assist chemical formulation of sunscreens and also to apprehend the way they protect, several modeling methods exist. Sunscreens are complex media that are usually modeled using the Beer-Lambert law [4–8] and Monte Carlo methods [9,10].

We propose other ways to model sunscreens, using electromagnetic calculations (Mie scattering, differential method, or scattering by a set of parallel cylinders). Unlike the models mentioned above, these electromagnetic calculations have a wide field of application: we can model chemical organic filters or mineral ones, on different substrates (*in vitro* or *in vivo*).

To do so, we have to image the cream distribution on a substrate. This knowledge allows us to compute the cream extinction using differential methods. These calculations have been compared to a model widely used in the sunscreen simulation field (step-film model [11]) in the case of chemical filters and measurements in the case of mineral filters.

Then, other methods using Mie theory or scattering by a set of parallel cylinders are used and compared to differential methods: depending on

the type of calculation desired, one or another method will be chosen. We conclude by giving some examples that illustrate the type of calculations we are able to handle.

2. Description of the System

In order to calculate the transmission of spread UV protection, the knowledge of optical and geometrical parameters is required.

A. Cream

A sunscreen is an emulsion of several phases, containing many ingredients such as filters (for example, phenylbenzimidazole sulfonic acid, octocrylene, avobenzene, or TiO_2), emulsifier (for instance, cetareth-20), solvent (such as water, oil, or butylen glycol) or preservative (for example, methylparaben or propylparaben).

Filters are the main compounds that provide the sunscreen efficiency. We can distinguish two types:

- The chemical ones (for example, octocrylene) that are organic molecules absorbing selectively ultraviolet light
- The mineral ones (such as TiO_2) that are inorganic particles that scatter and may absorb some of UV radiation (Fig. 1).

Creams are usually emulsions but we assume that the water evaporates as the cream is spread. Thus, the medium surrounding the particles is considered homogeneous.

B. Substrate

The sunscreen is mostly spread on two kinds of substrates (Fig. 2):

- The skin and its uppermost layer, the stratum corneum, is the substrate used to determine the sunblock efficiency [the sun protection factor (SPF)].
- The poly(methyl methacrylate) (PMMA) substrate is used to determine an evaluation of the SPF *in vitro*.

As we can see (Fig. 2), the skin and PMMA substrate do not have the same roughness: skin is constituted of large plateaus separated by furrows of variable but large depths, whereas PMMA plates are a more granular substrates [5]. For easier

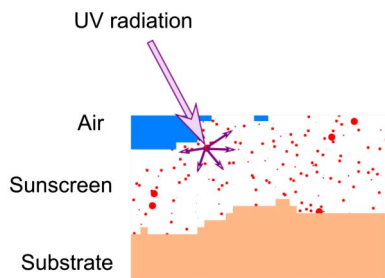


Fig. 1. Principle of UV protection by light scattering: UV radiations are scattered in all directions. The transmitted light loses energy by traveling a longer path, being reflected, or being absorbed by particles.

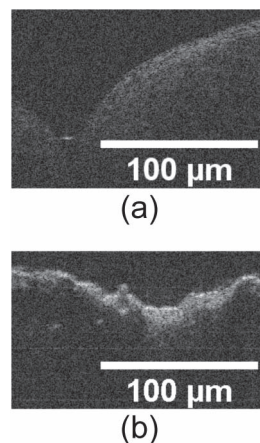


Fig. 2. Image of (a) a stratum corneum from abdomen, and (b) a PMMA plate, obtained by optical coherence tomography (OCT).

comparison with experimental data, we choose to model the transmission of a spread amount of sunscreen (1.2 mg/cm^2) on a PMMA substrate (purchased from Helioscience).

C. Sunscreen Efficiency Measurements

The SPF gives an indication of UV protection *in vivo*. It consists of the measurement of the amount of UV radiation required to cause sunburn on skin with the sunscreen on, as a multiple of the amount required without the sunscreen [12]. To compare sunscreens *in vitro*, a method has been developed using a substrate [4]. This method consists of a measurement of the transmission of the sunscreen applied on a substrate using a spectrometer (Fig. 3).

The spectrometer measures the quantity of light arriving in the integrating sphere. The light scattered by the sample (especially by the inorganic particles) is consequently taken into account. The wavelengths studied by this method are between 290 and 400 nm. Note that the whole transmitted light does not arrive in the integrating sphere, depending on the distance between the sample and the sphere but also of the size of sphere entrance. The characteristics of the setup used in this paper are detailed in Fig. 3.

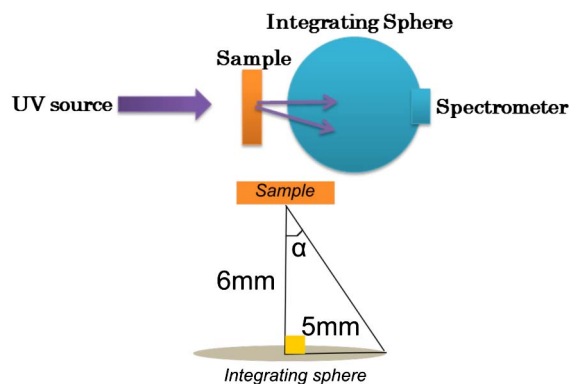


Fig. 3. Description of the sunscreen efficiency measurement *in vitro* and characteristics of the setup used. The angle α , representing the maximum scattered angle measured, is thus nearly equal to 40° .

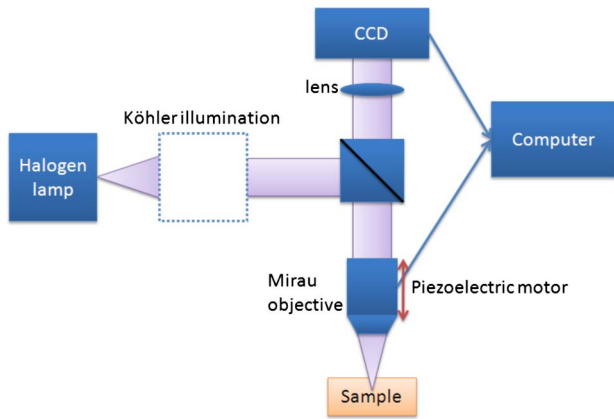


Fig. 4. Description of the OCT device used in this paper.

D. Evaluation of the Sunscreen Distribution

In order to evaluate the sunscreen distribution on the substrate, we choose to image the sunscreen applied on a PMMA plate using an optical coherence tomography (OCT) device (Fig. 4). The CCD and the piezoelectric motor allow us to image the sample in three dimensions.

An OCT image of a sunscreen applied (1.2 mg/cm²) on a PMMA plate directly (Fig. 5) does not allow us to know the distribution of the sunscreen.

The optical index contrast between the cream and the substrate is very low because their refractive indices are similar: the refractive index of the PMMA is 1.49 and the sunscreen is typically between 1.4 and 1.5 (depending on the oil used).

In order to distinguish this interface, we deposit a metallic thin film (thickness around 20 nm) on the PMMA before applying the sunscreen. Thus the interface between the cream and the substrate is clearly visible on the images (Fig. 6).

These images allow us to know precisely the distribution of the sunscreen on the substrate (Figs. 7 and 8).

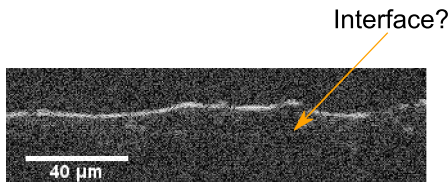


Fig. 5. OCT image of a sunscreen applied on a PMMA plate.

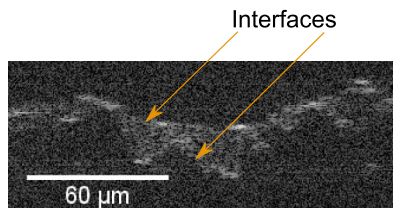


Fig. 6. OCT image of a sunscreen applied on a PMMA plate after the spread of a metallic thin film on the substrate.

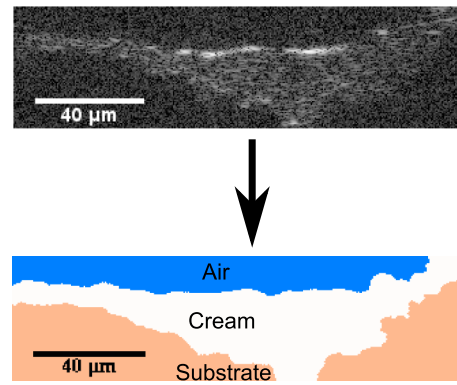


Fig. 7. Passage from an OCT image to a computable sunscreen distribution. In the case of chemical filters, the sunscreen is supposed homogeneous.

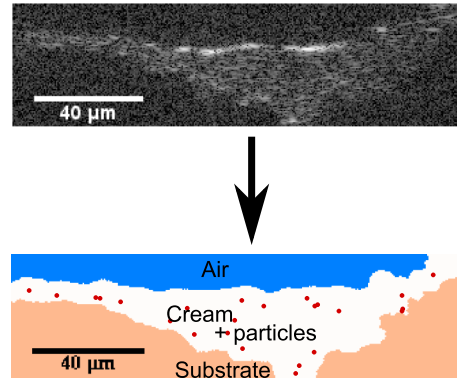


Fig. 8. Passage from an OCT image to a computable sunscreen distribution. If the filters are particles, they are represented by disks (red disks in the figure).

This distribution will be used to determine the sunscreen efficiency, using an electromagnetic calculation model.

3. Models of a Chemical Filters Sunscreen

A. Step-Film Model

In order to anticipate the transmission of the cream on the PMMA substrate, a model is widely used: the so-called step-film model [4–8].

This model does not take into account any inhomogeneity into the cream; therefore, it is particularly adapted to chemical creams.

Considering $I(\lambda, X)$ the intensity of the transmitted light, $I_0(\lambda)$ of the incident light, α the absorption coefficient, and X the length of the optical path, the Beer-Lambert law can be written:

$$I(\lambda, X) = I_0(\lambda) \exp(-\alpha X). \quad (1)$$

The idea of this model is to consider the cream as an homogeneous absorber (α do not depend on the position) with a nonuniform distribution on the substrate (the optical path X varies). The simplest step-film model consists of two different thicknesses [4] (Fig. 9). For each thickness X_1 and X_2 , a sunscreen quantity normalized F_1 and F_2 is associated.

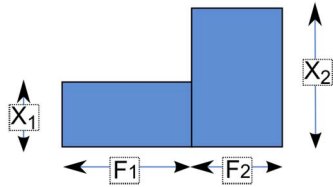


Fig. 9. Description of the step-film model.

In that case, the transmission $T = I/I_0$ is written

$$T = F_1 \exp(-\alpha X_1) + F_2 \exp(-\alpha X_2). \quad (2)$$

This model can be more accurate by taking into account not only two different thicknesses but an infinity number of it [6]. The values of the quantities F associated correspond to the distribution of the sunscreen on the substrate. Ferrero *et al.* [6] have chosen to write the function X depending on F as a gamma function, and have determined the coefficients by comparing the transmission of the model and the measured one.

The BASF Simulator [11], based on the step-film model can, for example, give the extinction of a chemical sunscreen (Fig. 10) using the following filters: 3% of avobenzone, 10% of octocrylene, and 1% of ensulizole.

Chemical filters can be degraded over time so the BASF Simulator calculates the extinction with the modification of α over time. This degradation, depending on the wavelength, will not be studied in this paper.

B. Differential Method: Model Description

In order to model a cream applied on a PMMA substrate measured by a spectrometer we use a differential method to solve Maxwell's equations. The method is fully described in other publications [12–14]. We consider three areas (Fig. 11). The superstrate (air) above the cream and the substrate below are assumed homogenous, linear, and isotropic.

In order to simplify the calculations, we assume that the structure is invariant along the y axis. This method is therefore a 2D method. The refractive

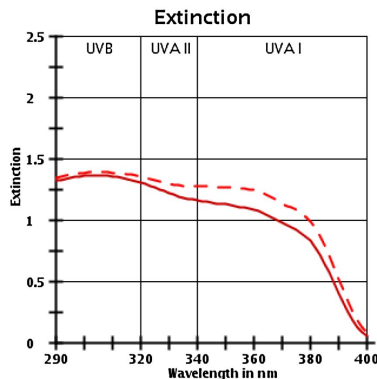


Fig. 10. Extinction of a chemical filters sunscreen using the step-film model. The dashed and the continuous red lines correspond respectively to the chemical compounds degraded and not degraded [11].

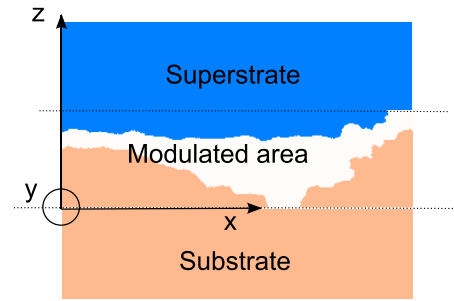


Fig. 11. Description of the three areas used in the differential method.

index of the modulated area is obtained from the OCT images. A detailed description of the differential method is beyond the scope of this paper but we give below a few basic elements of the theory.

The incident light is assumed to be a plane wave. We choose to calculate the transmission for transverse electric waves for normal incidence, but the transverse magnetic waves and others incidences are also computable.

\mathbf{E} is the electric field so the Helmholtz equation is written as

$$\Delta \mathbf{E} + k^2(x, z) \mathbf{E} = 0, \quad (3)$$

where k is the wavenumber,

$$k = \frac{2\pi n}{\lambda}, \quad (4)$$

with n the refractive index at the point considered, and λ the wavelength.

Given the structure geometry, Eq. (3) can be written as

$$\frac{\partial^2}{\partial z^2} \mathbf{E}_y(x, z) = -\frac{\partial^2}{\partial x^2} \mathbf{E}_y(x, z) - k^2(x, z) \mathbf{E}_y(x, z). \quad (5)$$

The Fourier transform of Eq. (5) gives

$$\frac{\partial^2}{\partial z^2} \hat{\mathbf{E}}_y(\sigma, z) = \sigma^2 \hat{\mathbf{E}}_y(\sigma, z) - k^2 \otimes \hat{\mathbf{E}}_y(\sigma, z). \quad (6)$$

We then discretize σ stating that $\sigma_\nu = \sigma_0 + \nu \Delta \sigma$, where $\nu < N$ is an integer. Note that it implies that we consider a periodic structure, i.e., a rough gratings whose period is given by Fig. 12. Thus, the diffracted far field consists of a discrete finite number of plane waves: the order of the gratings.

Equation (6), after being discretized, can be rewritten as a matrix equation:

$$[V(z)] = T(z, z')[V(z')], \quad (7)$$

where $[V(z)]$ is a matrix containing the vectors $\hat{\mathbf{E}}$ and $(\partial^2/\partial z^2) \hat{\mathbf{E}}$. T can be calculated using Runge–Kutta algorithm.

We then calculate the sum of the transmitted efficiencies, where an efficiency associated to a diffracted order corresponds to the Poynting flux

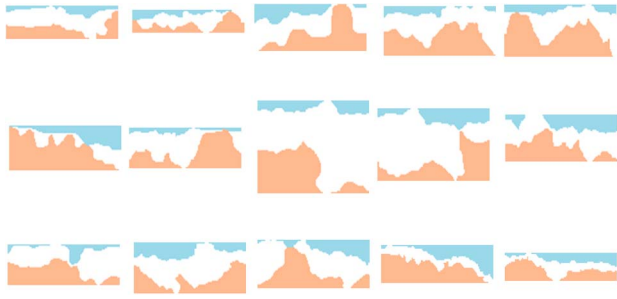


Fig. 12. Cross-cuts from 55 μm long OCT images. The air is represented in blue, the sunscreen in white, and the substrate (PMMA plate) in salmon color.

through a parallel surface of the modulated area, divided by the incident flux through the same surface.

C. Cream Distribution

Substantial differences can be observed depending on the location on the image: the distribution and the quantity of cream are not the same on all the areas on the PMMA plate [15]. In Fig. 12, we can find a representative set of cream repartitions obtained from OCT images.

From images of each area, we can calculate the extinction. Depending on the cross-cut the extinction can evolve from 1 to 10 times its minimum value.

We calculate the transmission of the 15 cross-cuts, and define the extinction using their mean value T . The extinction is defined by $E = -\log(T)$. We verified that the set of 15 cross-cuts is representative since we get the same E using another set of cross-cuts.

D. Comparison between the Differential Method and the Step-Film Model

In order to validate this numerical model, we compare the results of the differential method to the step-film model.

According to the results obtained (Fig. 13), the calculations using the differential method fit the

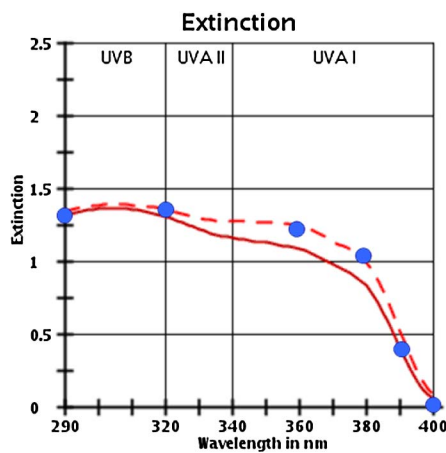


Fig. 13. Comparison between sunscreen simulator results and simulations using the differential method. The dashed and the continuous red lines correspond to the step-film model (with chemicals compounds degraded and not degraded, respectively) [11]. The blue points correspond to the results of the differential method simulations.

step-film model. This means that the cream distribution evaluated by the OCT device (Fig. 12) leads to a proper model.

4. Models of Sunscreen Containing Particles

A. Step-Film Model and Differential Method

Particles scatter and may absorb some of the light, that is why they are also used as UV filters (Fig. 1). The differential method, previously described, can be used to calculate the scattering of light through the whole system, placing particles inside the modulated area (Fig. 14).

In order to validate the differential method simulations, we compare the results obtained by the differential method and measurements. We choose a mineral sunscreen containing 10% of TiO_2 (HOMBITAN, from FF-Pharma [16]). The particles are randomly distributed and we calculate the extinction (Fig. 15).

It is worth noting that the differential method allows us to fit properly the experimental results while the step-film model results show clear discrepancies.

We will distinguish two regimes of scattering (Fig. 16):

- Single scattering: there is usually no interaction between the particles. It is the case if we have few

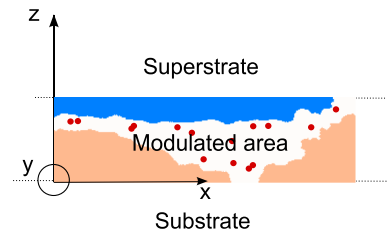


Fig. 14. Description of the three areas used in the differential method. The modulated area contains particles.

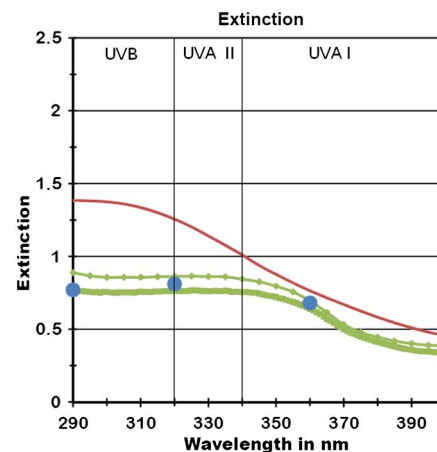


Fig. 15. Extinction of a mineral sunscreen. The green lines correspond to spectrometer measurements on two different samples. The blue points correspond to the results of simulations using the differential method. The step-film model (represented by the red line) did not match the measurements.

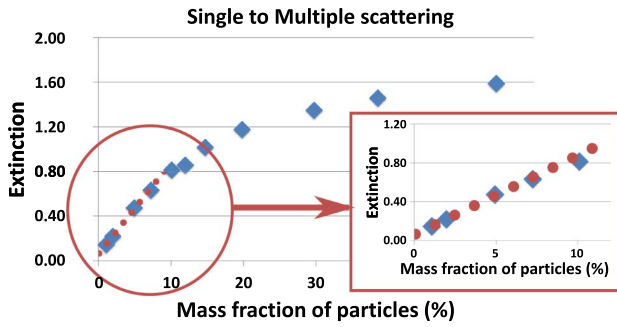


Fig. 16. Extinction as a function of the particles quantity, for TiO₂ spheres (diameter of 160 nm) and a wavelength of 310 nm. The blue points are calculated using the differential method whereas the red points correspond to single scattering; that is to say, the extinction is linearly dependent on the concentration of particles. Above 10% of mass fraction of particles multiple scattering become significant.

particles; the extinction is proportional to the quantity of particles.

- Multiple scattering: the light scattered by a particle can be scattered again by another particle. The extinction is no longer proportional to the quantity of particles.

In the case of single scattering, the Beer–Lambert law [Eq. (1)] can be used: the extinction is proportional to the quantity of particles.

Note that the wavelength, the material, or the diameter of the particles change the limit of validity of the models that do not take into account multiple scattering. It also modifies the effective coefficient α of the Beer–Lambert law. Electromagnetic models are consequently more appropriate in order to study several kinds of particles at any wavelength or concentration.

Nevertheless, the differential method leads to two substantial drawbacks:

- It is a rather slow method. Thus, it is practically limited to 2D models for our purpose. Taking a computer of 320 Go of RAM and an AMD processor (2.3 GHz), the time calculation, at a wavelength of 290 nm, is 130 h.

- Every type of particle (for example metals) cannot be modeled. For example, metallic particles require 3D models.

Therefore, we describe others methods to model the particles.

B. Scattering by a Set of Parallel Cylinders

We will present a numerical method based on cylindrical Bessel function development of the electromagnetic fields around cylinders. It allows us to compute the scattering of light by a set of parallel cylinders.

We consider a set of parallel cylinders, all included in a larger cylinder \mathcal{D} (Fig. 17).

In the following lines, we give a sketch of the method [17,18], assuming for simplicity that the \mathbf{E} field is parallel to the cylinders.

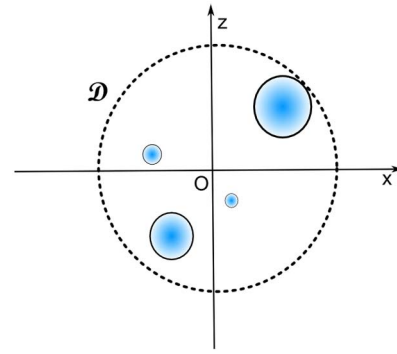


Fig. 17. Description of the scattering by a set of parallel cylinders.

Around each cylinder, the field can be written as a Fourier–Bessel development in the form

$$\mathbf{E} = \sum_{\nu \in \mathbb{Z}} (A_{\nu} J_{\nu}(kr) + B_{\nu} H_{\nu}^{(1)}(kr)) \exp(i\nu\theta), \quad (8)$$

where r and θ are the coordinates in the local system attached to the cylinder, A_{ν} and B_{ν} are the coefficients of the incident and scattered fields on the cylinder.

The relationship between the B_{ν} and A_{ν} coefficients is given by the scattering matrix of each cylinder that express trivially for cylinders with circular cross section.

The field scattered by each cylinder must be considered as an incident field upon all the other cylinders. The translation's formulas for Bessel functions (Graf's addition theorem) allow us to take it into account conveniently.

This leads to a linear system. The second member is entirely given by the knowledge of the external incident field on the whole structure. Solving the system gives the B_{ν} and A_{ν} coefficients for each cylinder. At this stage the field and the Poynting vector can be computed everywhere.

This method does not take into account the air-cream and the cream–substrate interfaces.

In order to use the calculation of the scattering by a set of parallel cylinders, we have to separate the influence of the cream and the interface. To do so, we calculate for the 15 images (Fig. 12), by the differential method, the transmission of the interfaces and the transmission of the cream alone. We then compare the transmission of the whole system to the transmission of the first interface (air/cream) multiplied by the transmission of the cream and the second interface (cream/substrate) (Fig. 18).

After having calculated the transmission through the decomposed system, we compared to the whole one. The error we found, defined by

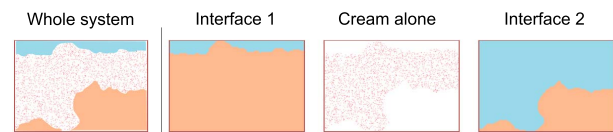


Fig. 18. Decomposition of the whole system to simplify our model.

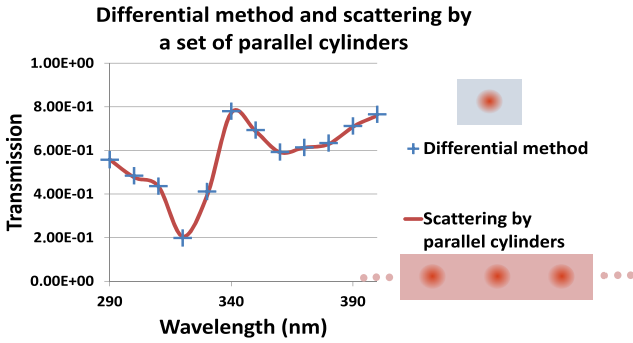


Fig. 19. Comparison between the differential method and scattering by parallel cylinders.

$(T_{\text{decomposedsystem}} - T_{\text{wholesystem}})/T_{\text{decomposedsystem}}$, was close to 2%.

We can also notice that if the cream is protective enough, the extinctions of the interfaces are negligible compared to the extinction of the cream alone.

The calculation by a set of parallel cylinders gives identical results to the differential method (Fig. 19) and has the advantage to work faster: for the same computer, instead of 130 h at the wavelength of 290 nm, it takes approximately 3 h.

C. Mie Scattering

Mie theory, describing the scattering of light by a sphere, is another possible approach. This method calculates the transmission of a single sphere inside a linear, homogeneous, and isotropic medium.

A solution of the Helmholtz equation [Eq. (3)], written in polar coordinates, can be expressed by separation of variables $f = f_1(R)f_2(\theta)f_3(\varphi)$, with f the electric or magnetic field, R the radial coordinate, θ and φ the angular coordinates, and k the wavenumber.

We obtain one equation per function:

- f_1 : a Bessel's equation
- f_2 : a Legendre's equation
- f_3 : an harmonic equation

Using these equations, the electric field E_s in the far field, can be expressed as [19,20]

$$E_s = E_0 \sum_{n=1}^{\infty} i^\nu \frac{2\nu + 1}{\nu(\nu + 1)} [\alpha_\nu^d \mathbf{M} - i b_\nu^d \mathbf{N}]. \quad (9)$$

E_s is the scattering field, E_0 the incident field, \mathbf{M} and \mathbf{N} are two vectors which can be expressed using the solutions of the equations of f_1, f_2 , and f_3 . α_ν^d and b_ν^d are constants whose depends on two key parameters:

$$q_1 = \frac{2\pi}{\lambda} n_1 a, \quad (10)$$

$$q_2 = \frac{2\pi}{\lambda} n_2 a, \quad (11)$$

where n_1 and n_2 are the refractive index of the particle and the medium, respectively, and a is the sphere radius.

As Mie scattering considers only one particle, we have to assume that there will not be any interaction between the particles; that is to say, we have to presume that only single scattering is involved. That is the case if we have few particles (Fig. 16). Multiple scattering can be expressed using several models, such as the multiple sphere T-matrix method [21] and the general multi-particle Mie [22]. We will not discuss these models in this paper.

If there is no multiple scattering, we can express the extinction of a bunch of particles using the extinction of one particle. To do so, we calculate a loss coefficient α , which will quantify the amount of lost energy light per nanometers:

$$\alpha = N\pi a^2(A + S), \quad (12)$$

where N is the number of particles per nm^3 , a the sphere radius, A the absorption of one particle, and S the backscattering of one particle. The α coefficient is then multiplied by every height of the images (expressed in nanometers) to obtain the global extinction.

We can compare the results obtained by Mie theory and the differential method (Figs. 20 and 21)

The results we obtain are close to the differential method, but it is limited to the case of single scattering, which can be restrictive. The advantage of Mie

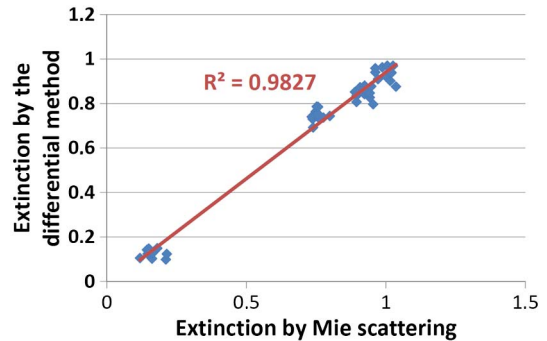


Fig. 20. Comparison between the extinction by the differential method and by Mie scattering. We verified that the mass fraction is below the multiple scattering point as we saw in Fig. 16. Note that Mie scattering is a 3D method whereas the differential method is a 2D one.

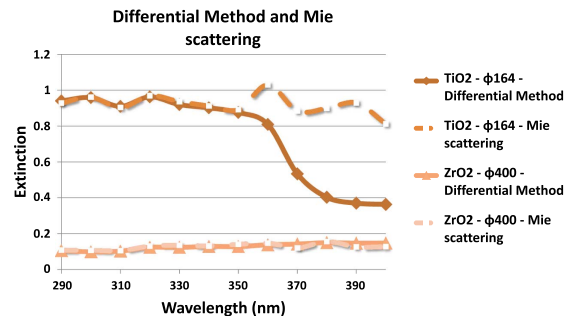


Fig. 21. Comparison between the extinction by the differential method and by Mie scattering for two particles. Above 350 nm TiO_2 particles scatters in multiple scattering, so the two methods do not match.

theory is the calculation time (with the same computer, it takes approximately 2 min at a wavelength of 290 nm). Moreover, this method is a 3D method, which is why it can model more type of materials (metals, for example). The results shown also validate that for dielectric particles a 2D model allows us to obtain qualitative extinction modeling.

5. Examples

We illustrate the methods described previously with specific examples.

A. Cream Distribution

The cream distribution is deduced from OCT cross-cuts. We have calculated the transmission using the images (Fig. 12).

We have also calculated the transmission of a cream perfectly distributed, which is to say the height of the sunscreen is a constant, regardless of the localization (Fig. 22). The height of the sunscreen is determined so that the quantity of cream is the same as in the distribution from OCT cross-cuts.

We can then calculate the sunscreen transmission by using the differential method or Beer-Lambert law. Note that Beer-Lambert law is faster but does not take into account the surface scattering. We obtain, using the differential method, a protection better in the case of a sunscreen perfectly distributed (Fig. 23).

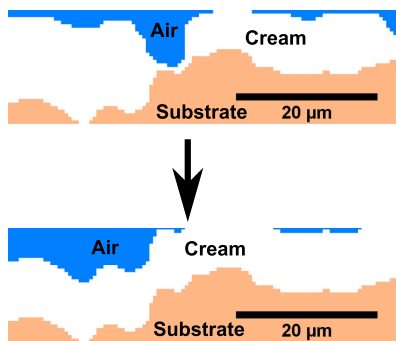


Fig. 22. Passage from a distribution obtained with a OCT cross-cut to a cream perfectly distributed.

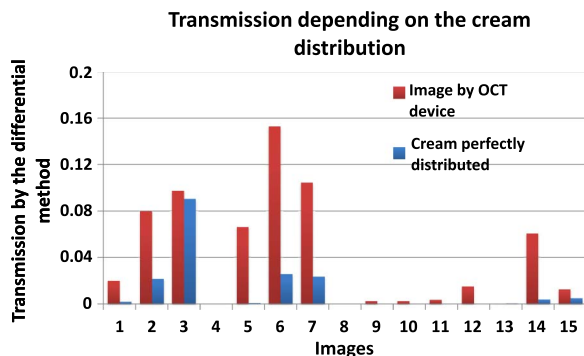


Fig. 23. Transmission, using the differential method, of the 15 images depending on the cream distribution. The wavelength is 320 nm and the sunscreen is the same as that used in Figs. 10 and 13.

The global extinction we obtain in our example is 1.39 in the case of the real sunscreen and 1.94 in the case of the cream perfectly distributed, showing the importance of the distribution of the cream. We can note (Fig. 23) that the transmission varies a lot from one image to another (from $2 \cdot 10^{-8}$ to 0.15). The standard deviation is equal to 0.05 in the case of images from the OCT device and 0.02 in a cream perfectly distributed.

B. Size of the Particles

When the filters are particles, the size of the scatterers is an important parameter: at a constant concentration, the size of the particles determines the number of particles (Fig. 24) but also changes the quantity of light scattered per particle.

Consequently, the UV protection varies with the particles diameters. We can calculate the variation by using the differential method or the scattering by a set of parallel cylinders (Fig. 25). The second method gives faster results.

C. Substrate

In order to measure the SPF *in vitro*, the sunscreen is applied on a PMMA plate. However, *in vivo*, the sunscreen is applied on the uppermost layer of the skin, the stratum corneum.

In order to model the extinction *in vivo*, we change the substrate. The PMMA plate is substituted by cells of the following refractive index: the cell interior is 1.34 whereas the intercellular matrix is 1.47 [23]. The absorption coefficient of the stratum corneum is

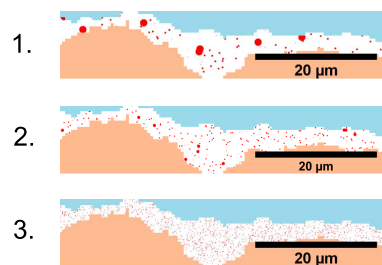


Fig. 24. Three images of the same quantity of TiO_2 but with different sizes. As we kept constant the concentration of TiO_2 , the number of scatterers is different.

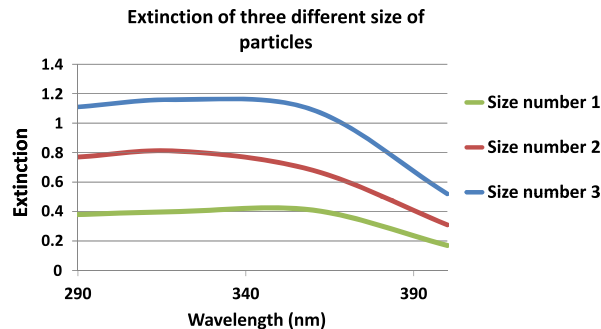


Fig. 25. Extinction of three particles of TiO_2 . Their sizes are described in Fig. 24.

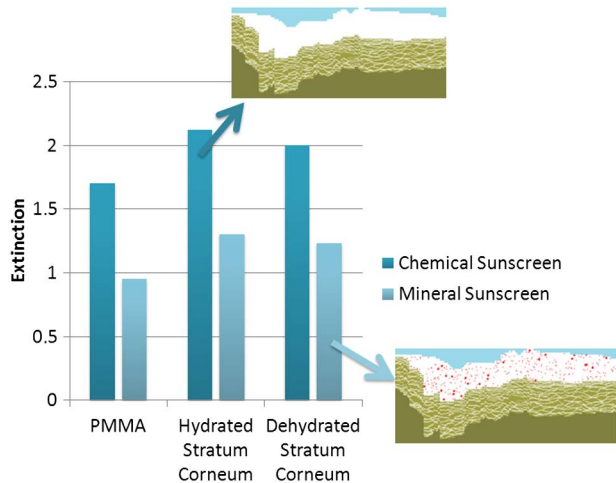


Fig. 26. Comparison of the extinction of two types of cream depending on the substrate at a wavelength of 320 nm. The chemical sunscreen is the same as that used in Figs. 10 and 13. The mineral sunscreen is the one used in Fig. 15.

approximately 60 mm^{-1} , and the imaginary part of the effective optical index is 0.0015 at a wavelength of 320 nm [9].

The images of the stratum corneum are provided by histological images, which may be different from an actual stratum corneum *in vivo*.

We can model the hydration or dehydration of the stratum corneum, by making the hypothesis that the hydration (or dehydration) results in a thickness increase (or resp. decrease) of the corneocytes of the stratum corneum [24]. The method used in that case is the differential method because this method can model variations of the substrate.

From Fig. 26 we notice that there is a small improvement of the extinction when the stratum corneum is hydrated.

6. Conclusion

We discussed several methods in order to model the sunscreen protection. The step-film model is the faster method, but does not take into account scattering by interfaces and particles. The differential method is a rigorous electromagnetic method and has been compared to the step-film model in simple cases of chemical sunscreens and to measurements in the case of mineral sunscreen.

However, each calculation using this method lasts particularly long and is practically limited to 2D structures, so every particle material cannot be modeled (especially the metals). Alternative methods, like Mie scattering (a 3D method) or the scattering of a set of parallel cylinders (a faster method) can be used.

The ensemble of modeling methods we have presented allows us to handle a large variety of sunscreens issues.

This study was supported by a grant from Naos Recherche.

References

1. M. F. Holick, "McCullum Award Lecture, 1994: vitamin D—new horizons for the 21st century," *Am. J. Clin. Nutr.* **60**, 619–630 (1994).
2. D. Wolpowitz and A. B. Gilchrist, "The vitamin D questions: how much do you need and how should you get it?" *J. Am. Acad. Dermatol.* **54**, 301–317 (2006).
3. V. N. Poochareon and C. J. Cockerell, "The war against skin cancer: the time for action is now," *Arch. Dermatol.* **141**, 499–501 (2005).
4. B. L. Diffey and J. Robson, "A new substrate to measure sunscreen protection factors throughout the ultraviolet spectrum," *J. Soc. Cosmet. Chem.* **40**, 127–133 (1989).
5. L. Ferrero, M. Pissavini, and O. Doucet, "How a calculated model of sunscreen film geometry can explain *in vitro* and *in vivo* SPF variation," *Photochem. Photobiol. Sci.* **9**, 540–551 (2010).
6. L. Ferrero, M. Pissavini, S. Marguerie, and L. Zastrow, "Efficiency of a continuous height distribution model of sunscreen film geometry to predict a realistic sun protection factor," *J. Cosmet. Sci.* **54**, 463–481 (2003).
7. D. F. Tunstall, "A mathematical approach for the analysis of *in vitro* sun protection factor measurements," *J. Cosmet. Sci.* **51**, 303–315 (2000).
8. B. Herzog, "Prediction of sun protection factors by calculation of transmissions with a calibrated step film model," *J. Cosmet. Sci.* **53**, 11–26 (2002).
9. A. P. Popov, A. V. Zvyagin, J. Lademann, M. S. Roberts, W. Wanchez, A. P. Priezzhev, and R. Myllyl, "Designing inorganic light-protective skin nanotechnology products," *J. Biomed. Nanotechnol.* **6**, 432–451 (2012).
10. A. P. Popov, J. Lademann, A. P. Priezzhev, and R. Myllyl, "Effect of size of TiO_2 nanoparticles embedded into stratum corneum on ultraviolet-A and ultraviolet-B sun-blocking properties of the skin," *J. Biomed. Opt.* **10**, 064037 (2005).
11. BASF, "Sunscreen simulator," http://www.sunscreensimulator.basf.com/Sunscreen_Simulator.
12. Food and Drug Administration (FDA), "Sunburn protection factor (SPF)" (2009).
13. L. Arnaud, G. Georges, C. Deumie, and C. Amra, "Discrimination of surface and bulk scattering of arbitrary level based on angle-resolved ellipsometry: theoretical analysis," *Opt. Commun.* **281**, 1739–1744 (2008).
14. M. Nevire and E. Popov, *Light Propagation in Periodic Media: Differential Theory and Design* (Mercel Dekker, 2002).
15. M. Pissavini, B. Diffey, S. Marguerie, T. Carayol, and O. Doucet, "Predicting the efficacy of sunscreens *in vivo* veritas," *Int. J. Cosmet. Sci.* **34**, 44–48 (2011).
16. http://www.kemi.com.mx/Hojas-Tecnicas/HOMBITAN_FF_PHARMA.pdf.
17. D. Felbacq, G. Tayeb, and D. Maystre, "Scattering by a random set of parallel cylinders," *J. Opt. Soc. Am. A* **11**, 2526–2538 (1994).
18. R. Petit, M. Cadilhac, D. Maystre, P. Vincent, M. Nevire, R. C. McPhedran, G. H. Derrick, and L. C. Botten, *Electromagnetic Theory of Gratings* (Springer-Verlag, 1980).
19. C. F. Bohren and D. R. Huffman, *Absorption and Scattering of Light by Small Particles* (Wiley-Blackwell, 1998).
20. H. C. van de Hulst, *Light Scattering by Small Particles* (Dover, 1982).
21. D. W. Mackowski and M. I. Mishchenko, "A multiple sphere T-matrix Fortran code for use on parallel computer clusters," *J. Quant. Spectrosc. Radiat. Transfer* **112**, 2182–2192 (2011).
22. Y. L. Xu, "Electromagnetic scattering by an aggregate of spheres: far field," *Appl. Opt.* **36**, 9496–9508 (1997).
23. R. Niesner, B. Peker, P. Schlüsche, K.-H. Gericke, C. Hoffmann, D. Hahne, and C. Müller-Goymann, "3D-resolved investigation of the pH gradient in artificial skin constructs by means of fluorescence lifetime imaging," *Pharm. Res.* **22**, 1079–1087 (2005).
24. J. A. Bouwtra, A. de Graaff, G. S. Gooris, J. Nijssse, J. W. Wiechers, and A. C. van Aelst, "Water distribution and related morphology in human stratum corneum at different hydration levels," *J. Invest. Dermatol.* **120**, 750–758 (2003).